Physical Measurement Laboratory: Spectroscopy

Ariel Whitehead,[1] Ashlee Jadloski,[1] and Chirag Gokani[1]
Department of Physics, University of Texas at Dallas, Richardson, Texas 75080, USA

(Dated: 7 December 2020)

We photographed and analyzed the spectra of 13 stars in the winter sky. The chosen stars varied in apparent magnitude and color, giving a broad distribution of absolute magnitude and spectral class. We studied the spectrum obtained for each star and identified peaks that correspond to the chemical composition of the star, similar to the Raman spectroscopy lab. We compared our results to those found in professional spectroscopy databases and journals.

In the heavens we discover [stars] by their light, and by their light alone…the sole evidence of the existence of these distant worlds…that each of them is built up of molecules of the same kinds we find on earth. A molecule of hydrogen, for example, whether in Sirius or in Arcturus, executes its vibrations in precisely the same time. Each molecule therefore throughout the universe bears impressed upon it the stamp of a metric system as distinctly as does the metre of the Archives at Paris, or the royal cubit of the Temple of Karnac.

—James Clerk Maxwell
Conduction of Electricity through Gases, 1873

I. HISTORY & SIGNIFICANCE

When Isaac Newton first passed sunlight through a prism, he used the term "spectrum" to describe the various emerging colors.[1] Advances in optics and observational astronomy in the 18th century set the stage for Joseph von Fraunhofer to famously re-analyze the spectrum of sunlight, revealing hundreds of absorption lines (so-called "Fraunhofer lines").[2] The origin of these lines, and the absorption and emission lines in other gases, sparked discussion among physicists and chemists for the next century, playing a major role in the development of quantum mechanics: see section (II).

Today, spectroscopy remains central to physics, astronomy, and chemistry, but its applications extend to biology, engineering, art history, forensics, and many other fields that explore the chemical composition of materials. Astronomical spectroscopy is particularly exciting because the spectra of stars and planets reveals more than just their composition. By analyzing how the spectra evolve in time, astronomers can map the dynamics of stellar rotation, binary star systems, exoplanets,[3] galactic rotation, and many other phenomena.

II. PHYSICAL DESCRIPTION

Since the spirit of our PML course is to appreciate the **physical reality** and **testability** of the many theories we have learned as undergraduates, we begin the technical portion of this report with a brief overview of the quantum mechanics, perturbation theory, and optics required to understand the physics of atomic spectra and spectroscopy.

A. Quantum mechanics explains spectra

While the Bohr model succeeded in predicting some prominent features of the spectra of hydrogen and hydrogen-like atoms, the origin of many other features remained unknown (ex., the fine structure of hydrogen, the 21-cm line, etc.). In the early 20th century, there were also unresolved problems in the classical theory of matter. Perhaps the most famous of these questions is, "Why does the electron (a charge undergoing the constant acceleration of uniform circular motion in the Bohr model) not spiral into the nucleus (as it is losing energy in the form of a magnetic field)?"

It was a combination of unresolved issues in spectroscopy and theoretical physics that led to the development of quantum mechanics. Quantum mechanics was cobbled together by many physicists in the early 20th century, but by the late 1920s, two major views had evolved: the Schrödinger picture (wave mechanics) and the Heisenberg picture (matrix mechanics). It took P.A.M. Dirac to show the connection between these pictures. Dirac introduced the bra-ket notation and showed that both the Schrödinger and Heisenberg picture respectively satisfy equations (1) and (2) below:[4]

$$i\hbar \frac{\partial |\Psi\rangle_S}{\partial t} = \mathscr{H} |\Psi\rangle_S \tag{1}$$

$$i\hbar \frac{\partial |\Psi\rangle_H}{\partial t} = -\mathscr{H} |\Psi\rangle_H \tag{2}$$

where $|\Psi\rangle_S$ denotes the Schrödinger state ket and $|\Psi\rangle_H$ denotes the Heisenberg state ket.[5] Since the theory of stimulated emission is most commonly explained in the Schrödinger picture, we will use equation (1) as our governing equation in the remainder of the introduction. We will also drop the subscript $_S$ since we have established that we are working in the Schrödinger picture.

If we are interested in understanding the structure of atoms, we should focus on the spatial distribution of electrons. We should therefore appeal to the the position operator $\mathscr{X}$, which has its own eigenvalue equation

$$\mathscr{X} |\vec{x}\rangle = \vec{x}' |\vec{x}\rangle \tag{3}$$

where $\vec{x}'$ is the Euclidean 3-vector of eigenvalues. Multiplying equation (1) by the position eigenbras $\langle \vec{x}|$ gives

$$i\hbar\langle\vec{x}|\frac{\partial|\Psi\rangle}{\partial t} = \langle\vec{x}|\mathscr{H}|\Psi\rangle \quad (4)$$

$$i\hbar\frac{\partial\langle\vec{x}|\Psi\rangle}{\partial t} = \mathscr{H}\langle\vec{x}|\Psi\rangle \quad (5)$$

We were able to move the position eigenbra through the time derivative on the left-hand-side because the Schrödinger eigenbras do not evolve in time. On the right-hand-side, we recall that $\mathscr{H} = \frac{\vec{p}^2}{2m} + V(\vec{x})$. Since $\langle x'|p^n|\Psi\rangle = (-i\hbar)^n\frac{\partial^n}{\partial x'^n}\langle x'|\Psi\rangle$ (a result shown early in Dr. Gartstein's QM1 course) and $\langle\vec{x}|V(\vec{x}) = \langle\vec{x}'|V(\vec{x}')$ (by equation 3), the right-hand-side of equation (5) becomes

$$-\left(\frac{\hbar^2}{2m}\right)\vec{\nabla}'^2\langle\vec{x}'|\Psi\rangle + V(\vec{x}')\langle\vec{x}'|\Psi\rangle$$

It is conventional to denote $\langle\vec{x}|\Psi\rangle$ (which is the element of a matrix-like object representing the state $|\Psi\rangle$ in the basis of position eigenkets) as the *wave function*, $\Psi(\vec{x}',t)$. Upon these considerations, equation (5) reads

$$i\hbar\frac{\partial}{\partial t}\Psi(\vec{x}',t) = -\left(\frac{\hbar^2}{2m}\right)\vec{\nabla}'^2\Psi(\vec{x}',t) + V(\vec{x}')\Psi(\vec{x}',t) \quad (6)$$

Equation (6) is what we most immediately recognize to be Schrödinger's time-dependent wave equation. This is a first-order partial differential equation in the Hilbert space that can be solved by separation of variables. For simplicity, we can drop the primes that denote eigenvalues. Writing the wave function $\Psi(\vec{x}',t)$ as the product of spatial and temporal functions $\psi(\vec{x})$ and $\phi(t)$, making some algebraic manipulations, and introducing a separation constant E, equation (6) becomes[6]

$$i\hbar\frac{1}{\phi(t)}\frac{\mathrm{d}\phi(t)}{\mathrm{d}t} = E = -\frac{\hbar^2}{2m}\frac{1}{\psi(\vec{x})}\vec{\nabla}^2\psi(\vec{x}) + V(\vec{x})$$

Solving the left-hand-side for $\frac{\mathrm{d}\phi}{\mathrm{d}t}$ gives

$$\frac{\mathrm{d}\phi}{\mathrm{d}t} = -\frac{iE}{\hbar}\phi$$

whose solution we immediately read off as

$$\phi(t) = \exp(-iEt/\hbar)$$

We see that $\phi(t)$ is just executing waves in complex space, and since we are more interested in the spatial structure of atoms, we often disregard the time-dependent factor of the solution when describing the eigenstates of atoms. Turning our attention to the more relevant right-hand-side,

$$-\frac{\hbar^2}{2m}\vec{\nabla}^2\psi(\vec{x}) + V(\vec{x})\psi(\vec{x}) = E\psi \quad (7)$$

we see that the solution of this equation depends on the given potential $V(\vec{x})$. It turns out that this equation can be solved analytically only for hydrogen, the simplest of atoms, whose potential is $V = -\frac{1}{4\pi\varepsilon_0}\frac{q}{x}$ where $x = |\vec{x}| = \sqrt{\sum_{i=1}^{3}x_i^2}$. We seek numerical solutions for all other atoms of atomic number $Z > 1$.

Solving equation (7) (which is really an eigenvalue equation $\mathscr{H}\psi_n = E_n\psi_n$) gives the full spectrum of energy eigenvalues E_n. When an electron transitions from a state with energy E_m to a state with energy E_n, energy in the form of electromagnetic radiation is released (for $m > n$). Since the energy eigenvalues are "spaced" differently for different atoms, the spectra that result from the transitions between the various energy eigenvalues serve as a way to uniquely identify atoms. By taking spectra of starlight and looking for prominent features that correspond to the spectra, we are able to identify the chemical composition of stars.

It is important to note that not all transitions are possible. The allowed transitions are determined by the theory of angular momentum. Specifically, transitions occur if the matrix element $\langle n'l'm'|\vec{r}|nlm\rangle \neq 0$. For this condition,[7] $\Delta m = \pm 1$ or 0 and $\Delta l = \pm 1$. These so-called "selection rules" give rise to distinct spectroscopic features.

B. Stimulated emission

In stellar spectroscopy, we look for **absorption lines**. The star is roughly a blackbody, emitting light at all frequencies, but elements in the photosphere of stars absorb light at particular frequencies determined by the chemical composition of the photosphere. This process of absorption is essentially the inverse of emission, so we discuss the process of emission below. The math is the same; just switch $m > n$ with $m < n$.

For simplicity,[8] let's assume there are only two (orthonormal) states, ψ_a and ψ_b, each the eigenstate of the Hamiltonian $\mathscr{H}^0$ with respective eigenvalues E_a and E_b. We can represent any state of this system as the linear combination of the stationary states:

$$\Psi(t) = c_a\psi_a e^{-iE_at/\hbar} + c_b\psi_b e^{-iE_bt/\hbar}$$

In the presence of a time-dependent perturbation $\mathscr{H}'(t)$, the coefficients become functions of time:

$$\Psi(t) = c_a(t)\psi_a e^{-iE_at/\hbar} + c_b(t)\psi_b e^{-iE_bt/\hbar} \quad (8)$$

These time-dependent coefficients can be found by imposing the time-dependent Schrödinger equation on $\Psi(t)$:

$$\mathscr{H}\Psi = i\hbar\frac{\partial\Psi}{\partial t} \quad (9)$$

where $\mathscr{H} = \mathscr{H}^0 + \mathscr{H}'(t)$. Putting together equations (8) and (9),

$$\begin{aligned} c_a(\mathscr{H}^0\psi_a)e^{-iE_at/\hbar} + c_b(\mathscr{H}^0\psi_b)e^{-iE_bt/\hbar} + \\ + c_a(\mathscr{H}'\psi_a)e^{-iE_at/\hbar} + c_b(\mathscr{H}'\psi_b)e^{-iE_bt/\hbar} \\ = i\hbar\dot{c}_a\psi_a e^{-iE_at/\hbar} + i\hbar\dot{c}_a\psi_a e^{-iE_at/\hbar} + \\ + i\hbar c_a\psi_a\left(-\frac{iE_a}{\hbar}\right) + i\hbar c_b\psi_b\left(-\frac{iE_b}{\hbar}\right) \end{aligned}$$

But since $\mathscr{H}^0\psi_a = E_a\psi_a$ and $\mathscr{H}^0\psi_b = E_b\psi_b$, the first two terms on the left-hand-side cancel with the last two terms on the right-hand-side, giving

$$\begin{aligned} c_a(\mathscr{H}'\psi_a)e^{-iE_at/\hbar} + c_b(\mathscr{H}'\psi_b)e^{-iE_bt/\hbar} \\ = i\hbar\left(\dot{c}_a\psi_a e^{-iE_at/\hbar} + \dot{c}_a\psi_a e^{-iE_at/\hbar}\right) \end{aligned}$$

Taking the inner product with ψ_a and noting $\langle\psi_a|\psi_b\rangle = 0$,

$$c_a\langle\psi_a|\mathscr{H}'|\psi_a\rangle e^{-iE_at/\hbar} + c_b\langle\psi_a|\mathscr{H}'|\psi_b\rangle e^{-iE_bt/\hbar} = i\hbar\dot{c}_a$$

Defining $\mathscr{H}'_{ij} \equiv \langle\psi_i|\mathscr{H}'|\psi_j\rangle$,

$$\dot{c}_a = -\frac{i}{\hbar}\left(c_aH'_{aa} + c_bH'_{ab}e^{i(E_b-E_a)t/\hbar}\right) \tag{10}$$

Similarly, taking the inner product with ψ_b gives $\dot{c}_a$:

$$\dot{c}_b = -\frac{i}{\hbar}\left(c_bH'_{bb} + c_aH'_{ba}e^{i(E_b-E_a)t/\hbar}\right) \tag{11}$$

Often, the diagonal elements of the matrix $\mathscr{H}'$ vanish, so equations (10) and (11) simplify to

$$\dot{c}_a = -\frac{i}{\hbar}H'_{ab}e^{i\omega_0t}c_b \tag{12}$$

$$\dot{c}_b = -\frac{i}{\hbar}H'_{ba}e^{i\omega_0t}c_a \tag{13}$$

where we define $\omega_0 \equiv \frac{E_b-E_a}{\hbar}$. Assuming $\mathscr{H}'$ is small, to first-order approximation,

$$\frac{\mathrm{d}c_a}{\mathrm{d}t} = 0 \implies c_a(t) = 1$$

so

$$\frac{\mathrm{d}c_b}{\mathrm{d}t} = -\frac{i}{\hbar}\mathscr{H}'_{ba}e^{i\omega_0t}$$

Integrating,

$$c_b = -\frac{i}{\hbar}\int_0^t H'_{ba}(t')e^{i\omega_0t'}\,\mathrm{d}t' \tag{14}$$

Since stars radiate light (i.e., electromagnetic radiation), we can assume a sinusoidal time dependence of the form

$$H'_{ab} = V_{ab}\cos\omega t$$

Putting the above into equation (14) gives

$$\begin{aligned} c_b(t) &\approx -\frac{i}{\hbar}V_{ba}\int_0^t \cos\omega t' e^{i\omega_0t'}\,\mathrm{d}t \\ &= -\frac{iV_{ba}}{2\hbar}\int_0^t\left(e^{i(\omega_0+\omega)t} + e^{i(\omega_0-\omega)t}\right)\mathrm{d}t' \\ &= -\frac{V_{ba}}{2\hbar}\left(\frac{e^{i(\omega+\omega_0)t}-1}{\omega_0+\omega} + \frac{e^{i(\omega-\omega_0)t}-1}{\omega_0-\omega}\right) \end{aligned}$$

Often the driving frequency ω is close to the transition frequency ω_0 ($\omega_0 + \omega \gg |\omega_0 - \omega|$). $c_b(t)$ is dominated by the second term in the brackets:

$$\begin{aligned} c_b(t) &\approx -\frac{V_{ba}}{2\hbar}\left(\frac{e^{i(\omega-\omega_0)t}-1}{\omega_0-\omega}\right) \\ &= -\frac{V_{ba}}{2\hbar}\frac{e^{i(\omega_0-\omega)t/2}}{\omega-\omega_0}\left(e^{i(\omega-\omega_0)t/2} - e^{-i(\omega-\omega_0)t/2}\right) \\ &= -i\frac{V_{ba}}{\hbar}\frac{\sin\left((\omega_0-\omega)t/2\right)}{\omega_0-\omega}e^{i(\omega_0-\omega)t/2} \end{aligned}$$

Of course only real quantities can be measured, so we take $|c_b(t)|^2$, the so-called **transition probability**:

$$P_{a\to b}(t) = |c_b(t)|^2 \approx \frac{V_{ba}^2}{\hbar^2}\frac{\sin^2\left((\omega_0-\omega)t/2\right)}{(\omega_0-\omega)^2} \tag{15}$$

This is the theoretical framework that explains stimulated emission (and inversely absorption), the phenomenon we study in spectroscopy. Several approximations were made leading to equation (15), but more exact calculations can be made numerically (i.e., accounting for more than two energy levels, assuming the driving frequency is not close to the transition frequency, etc.).

Of course, none of these calculations are needed in the experimental science of spectroscopy, but we have presented them in the spirit of PML: to unite the theoretical understanding we have developed the past three years with hands-on experience.

C. Diffraction grating

A prism spreads light into the spectrum because different colors have different indexes of refraction; a diffraction grating achieves the same goal by making light travel different paths. Successive mirrors or (in our case) prisms are used to create a path difference $\Delta S = d(\sin\alpha \pm \sin\beta)$, where α and β denote the angles sketched in Figure I. The reflected or refracted light interferes constructively and destructively, with

the size of the diffraction pattern determined by the wavelength of light. Thus light of the similar wavelengths“bunch up," while light of dissimilar wavelengths cancel out. The result is the separation of light into the spectrum.

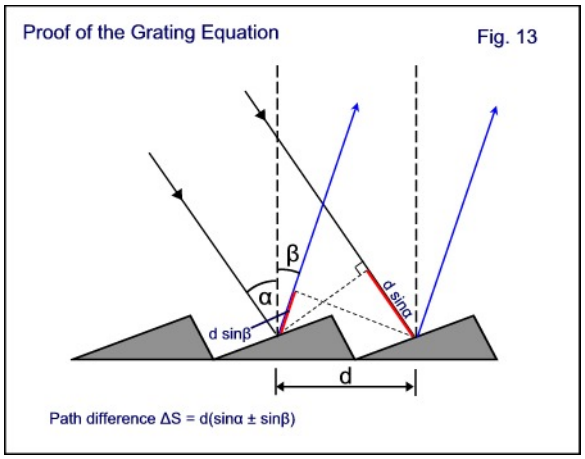

Figure I.[9] This schematic shows the geometry of a diffraction grating. In this diagram, successive mirrors create a path difference $\Delta S = d(\sin\alpha \pm \sin\beta)$, resulting in a diffraction pattern. The size of the diffraction pattern depends on wavelength of light. Thus light of different colors “bunches up" at different locations, resulting in a spectrum.

III. EXPERIMENTAL SETUP

A. Equipment

1. *Telescope*

While C.G. has extensive experience using UTD’s Celestron 8” Schmidt-Cassegrain telescope and checked the telescope out early October, he thought using his personal Tasco Newtonian reflector would be more convenient and appropriate for this project. Using this smaller telescope allowed for a faster set-up and break-down when on site. The smaller telescope also provided a more appropriate window in which the full spectrum could be captured.

2. *Diffraction grating*

UTD alumnus Ian Grey graciously let our team borrow his fine diffraction grating filter. It is a Paton Hawksley Education star analyzer diffraction grating valued at $250+.

3. *CCD*

In the early days of spectroscopy, spectra were recorded by analog means and analyzed visually. We are fortunate to have access to the appropriate technology with UTD’s CCD attachment and corresponding USB cable. The CCD is a ZWO ASI224MC camera. The CCD camera essentially functioned as a photometer, counting the number of photons per pixel. The photons per pixel data was then converted to an intensity vs. wavelength graph in `RSpec` (the full process of calibration can be found **here**).

4. *Software*

We used `SharpCap`, a free astronomy imaging software, to capture the spectra of the stars. The data was analyzed in `RSpec`, an expensive ($\sim$ $200) but very nice program that Chirag purchased upon recommendation from Ian Grey. Two drivers needed to be installed to have these programs register the ZWO ASI224MC camera. There was a broken link in RSpec’s instructions, but Chirag found the correct link, installed the drivers, and emailed Tom Field, President of RSpec, about the issue. Future releases of RSpec will have the correct address to the drivers linked.

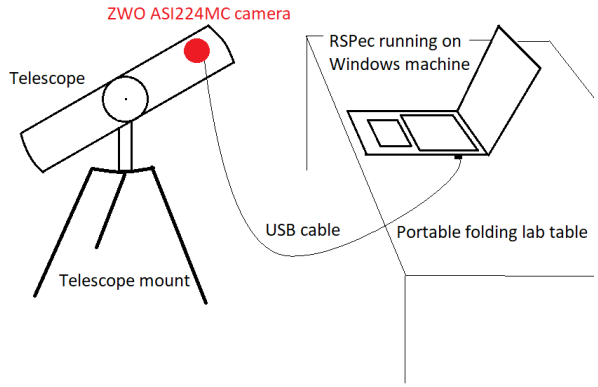

Figure II. Above is a schematic of our experimental setup. Perhaps the hardest part was aligning the telescope on the appropriate star. Since the Tasco Newtonian reflector telescope rests on a manual altitude-azimuth mount, making minor adjustments are challenging. Aligning the telescope to properly display the star and the associated spectrum required two people, since one person needs to be looking through the telescope’s view finder while the other needs to assess the position on computer screen.

B. Location

Accessing dark skies free of light-pollution is critical to any aspect of observational astronomy. Earlier this semester, C.G. scouted out a **dark site** that is northwest of Ft. Worth (a public park near the small town of Alvord). The park is at a slight elevation with few trees, providing an unobstructed of the sky. It is a quiet park with very little exposure to surrounding street lighting. This area is also far enough away from DFW to provide skies with relatively little light pollution. From past experience at this site, Chirag knew there is some pollution in the southwestern sky (the direction of DFW) but that this would not interfere significantly since most objects will be observed close to the zenith.

Our opportunities actually expanded when Chirag went to the mountains in northern New Mexico for two weeks in November. He brought with him all the equipment described in section (III A). The skies were stunningly clear, and the moon was below the horizon at sunset for the first few days Chirag was there, making for ideal observing conditions. Unfortunately, Chirag struggled with keeping the telescope focused and steady in the strong winds. Moreover, it was unbelievably cold (near 0° F for these nights, making observation very grueling. So, Chirag ended up collecting the data from his **parents' front yard** when he returned to Dallas.

IV. SPECTRA & COMPARISON TO LITERATURE

In this section, we analyze the spectrum obtained for each star and identify peaks that correspond to the chemical composition of the star. The form of our analysis is similar to the Raman spectroscopy lab. The stars are organized by the constellation to which they belong. The constellations are presented in their west-to-east order in the night sky.

For the sake of demonstration, the authors would like to present a raw image of the spectrum of the star we analyze in section (IV C 1), Betelgeuse. This is what Chirag saw on his laptop monitor while aiming the telescope on Betelgeuse:

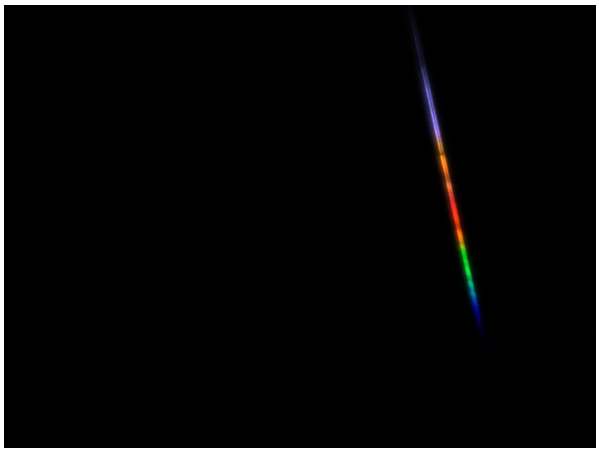

Zooming into this figure, you can see several large absorption lines visible. The figure is cropped down to the narrow strip of the spectrum, and then rotated counterclockwise by $\sim 75°$ to be horizontal. This rotated and cropped image is then processed in `RSpec`, where the photon count vs. pixel graph is constructed. The photons per pixel data is then converted to an intensity vs. wavelength graph in `RSpec`, which is what we juxtapose by the spectra from literature below.

A. Taurus

1. *Aldeberan (α-Tauri)*

Kaler notes that "Aldebaran's iron content (relative to hydrogen) is about half that of the Sun's,"[10] but that it is rich in carbon and oxygen. We were able to find three features in Aldeberan's spectrum characteristic of carbon.

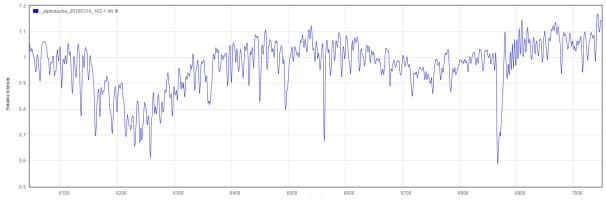

Figure III.[11] Above is a portion of the spectrum of Aldeberan found on the British Astronomical Association's database. The absorption line at 6122.00 Å helped us calibrate our own spectrum displayed below.

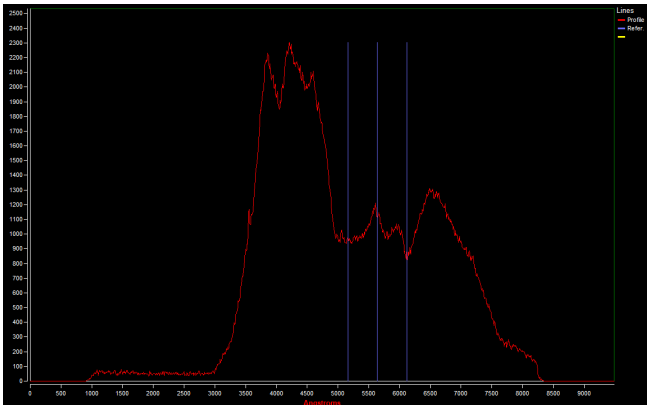

Figure IV. Above is our spectrum of Aldeberan. Absorption lines found at 5165.00, 5635.00, and 6122.00 Å correspond to carbon.

2. *Elnath (β-Tauri)*

Kaler calls Elnath "chemically peculiar," identifying it as a "mercury-manganese" star, like Alpheratz.[12] We were able to identify the same six absorption lines characteristic of mercury that we identified in Alpheratz in section (IV B 1).

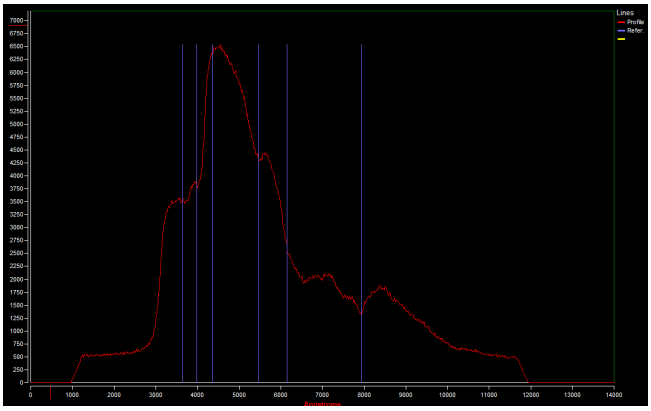

Figure V. Above is our spectrum of Elnath. We observed mercury absorption lines at 3650.15, 3983.93, 4358.33, 5460.74, 6149.48, and 7944.54 Å

B. Andromeda

1. *Alpheratz (α-Andromedae)*

According to Jim Kaler's extensive "Stars" database,[13] Alpheratz is particularly abundant in mercury manganese (in fact, it is the brightest so-called "mercury-manganese" star in the night sky). According to Kaler, "the atmosphere of these stars have vast enrichments of these elements, mercury over-abundant by a factor of tens of thousands."[14] We observed six absorption lines that correspond to the presence of mercury in the photosphere of Alpheratz.

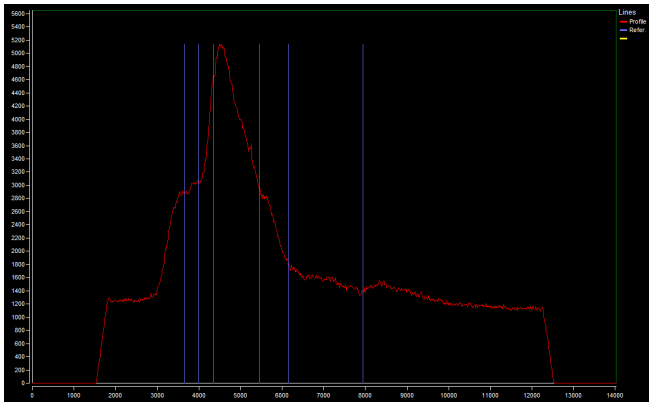

Figure VI. Above is our spectrum of Alpheratz. Six absorption lines at wavelengths 3650.15, 3983.93, 4358.33, 5460.74, 6149.48, and 7944.54 Å were observed and are overlaid (zoom in to see the blue lines) above the spectrum (the red line). These absorption lines correspond to the various energy transitions characteristic of mercury.

C. Orion

1. *Betelgeuse (α-Orionis)*

Betelgeuse is perhaps the most spectacular spectrum we measured (likely coincidental as Chirag was experimenting with the focus and exposure while taking this measurement). Spectra from literature (like the one shown below) show a predominance of hydrogen Balmer lines.

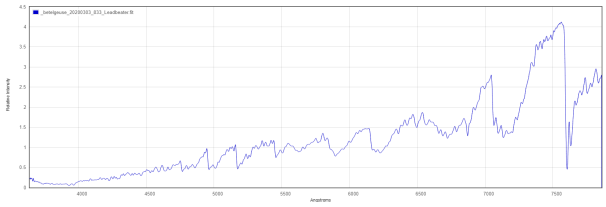

Figure VII.[15] Above is the spectrum of Betelgeuse found on the British Astronomical Association's database. We see signatures of hydrogen absorption, confirmed by the five hydrogen absorption lines obsved in our spectrum below.

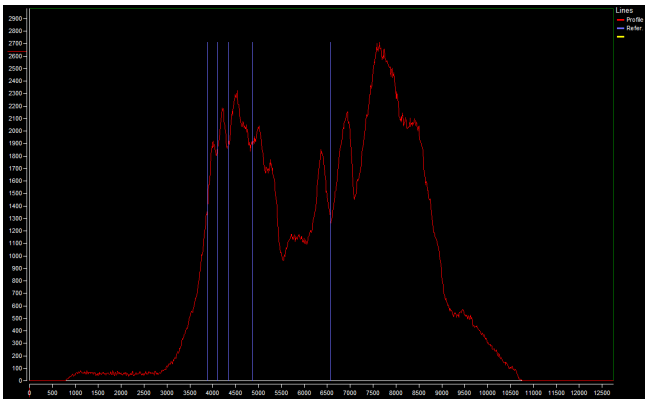

Figure VIII. Above is our spectrum of Betelgeuse. Absorption lines corresponding to Hydrogen Balmer transitions were observed at 3889.05, 4101.74, 4340.47, 4861.33, and 6562.81 Å.

2. *Rigel (β-Orionis)*

Rigel, a main-sequence class B star, is characterized by the process that drives all main-sequence stars: the fusion of four hydrogen atoms into a helium atom.[16] We therefore should expect a heavy presence of hydrogen Balmer lines in Rigel's spectrum.

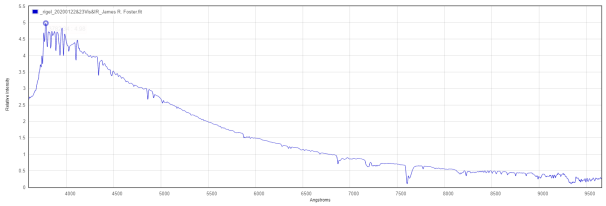

Figure IX.[17] Above is the spectrum of Rigel found on the British Astronomical Association's database. We see several lines in the 4000-6000 Å range that are characteristic of hydrogen Balmer lines.

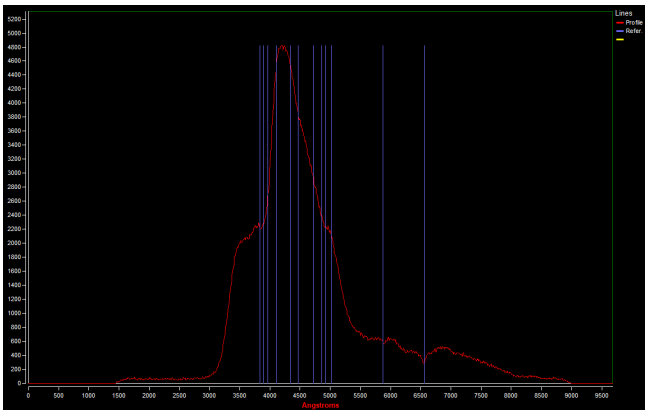

Figure X. Above is our spectrum of Rigel. We observed seven absorption lines at 3835.38, 3889.05, 3970.07, 4101.74, 4340.47, 4861.33, and 6562.81 Å corresponding to hydrogen Balmer absorption.

3. *Bellatrix (γ-Orionis)*

Bellatrix is classified as a hydrogen-fusing B2 star[18], and we therefore expect the predominance of hydrogen and helium absorption lines in its spectrum. While the hydrogen lines were harder to spot (we found three), the helium lines were easier to point out (we saw four).

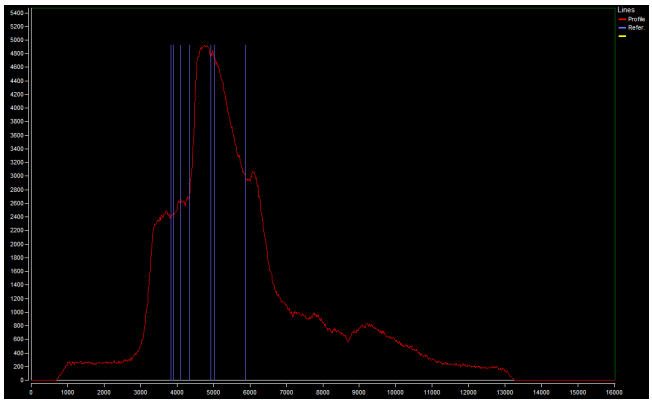

Figure XI. Above is our spectrum of Bellatrix. We saw three hydrogen Balmer lines at 3835.38, 4101.74, and 4340.47 Å, as well as four helium absorption lines at 3888.00, 4921.00, 5015.00, and 5875.00 Å.

4. *Mintaka (δ-Orionis)*

Like Bellatrix, Mintaka (a member of Orion's famous belt) is a type B star.[19] It is actually a double star, but its companion is too faint to be detected by our team's amateur equipment. As was the case for Bellatrix, we should look for hydrogen and helium lines.

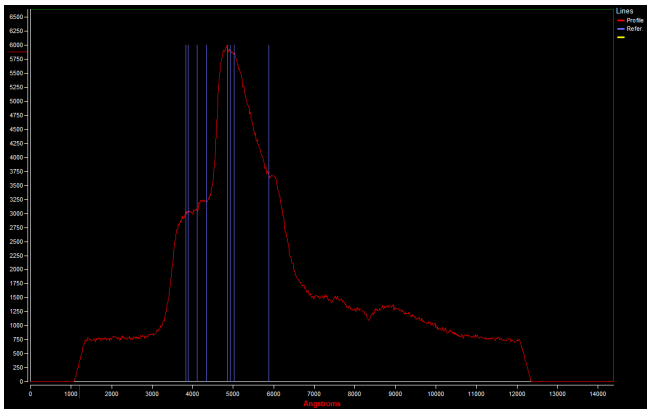

Figure XII. Above is our spectrum of Mintaka. We saw four absorption lines at 3835.38, 4101.74, 4340.47, and 4861.33 Å, corresponding to hydrogen Balmer lines. We also see four absorption lines at 3888.00, 4921.00, 5015.00, and 5875.00 Å, corresponding to helium absorption lines.

5. *Alnilam (ε-Orionis)*

Alnilam, the most luminous member of Orion's belt, is also a type-B star, though its hydrogen fusing stage is nearly over.[20] We should therefore expect a significant portion of its spectral features to reflect the presence of helium. We indeed observed four absorption lines due to hydrogen and four absorption lines due to helium.

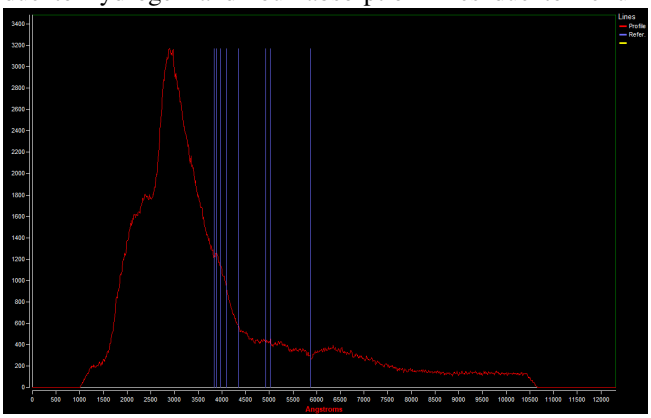

Figure XIII. Above is our spectrum of Alnilam. We observed absorption lines at 3835.38, 3970.07, 4101.74, and 4340.47 Å, corresponding to hydrogen Balmer absorption. We also observed absorption lines at 3888.00, 4921.00, 5015.00, and 5875.00 Å, corresponding to helium absorption.

6. *Alnitak (ζ-Orionis)*

Alnitak, the third member of Orion's belt, shares the spectral class of its two friends Alnilam and Mintaka: type-B.[21] It has begun its move off the main sequence, preceding Alnilam, and hydrogen fusion in its core has stopped. This particular spectra was difficult to analyze, mainly because the profile was rather "smooth" (i.e., there were few discernable features). We were expecting to see more telling signs of the presence of helium, but we only found two absorption lines that correspond to helium.

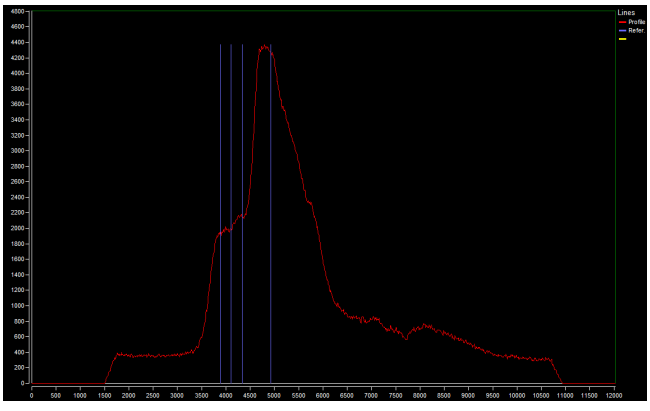

Figure XIV. Above is our spectrum of Alnitak. The absorption lines at 4101.74 and 4340.47 Å correspond to the presence of hydrogen, while the absorption lines at 3888.00 and 4921.00 Å correspond to the presence of helium.

The results for Alnitak are tenuous, and we will discuss various sources of errors leading to the weak features in section (V).

D. Auriga

1. Capella (α-Aurigae)

Capella, the leading light of Auriga, is perhaps the most difficult spectrum to interpret, as the single “star" we refer to as Capella is actually consists of five gravitationally bound stars.[22] Since the two largest members of this system, Capella Aa and Capella Ab, are both aging type-A stars, we expect a predominance of hydrogen and helium features in the spectra. We found four hydrogen absorption lines and two helium lines.

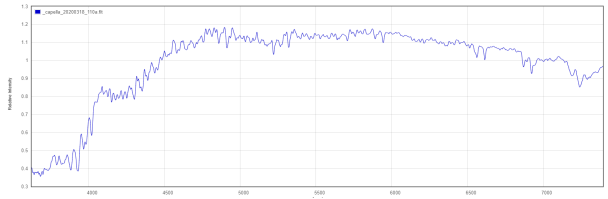

Figure XV.[23] Above is the spectrum of Capella found on the British Astronomical Association’s database. The spectrum’s features are subtle, making it difficult to interpret. Our spectrum (below), however, had prominent absorption lines in locations characteristic of hydrogen.

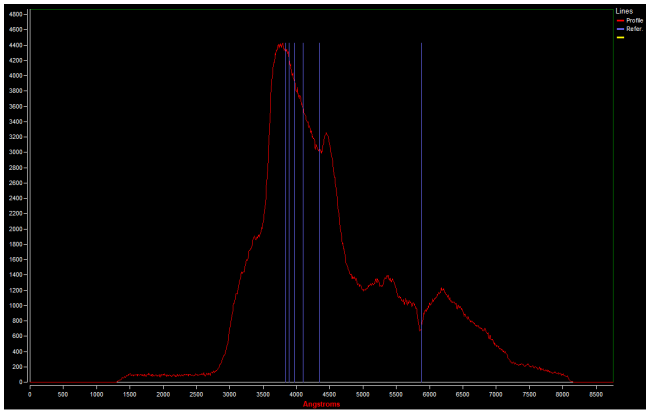

Figure XVI. Above is our spectrum of Capella. We saw absorption lines at 3835.38, 3970.07, 4101.74, and 4340.47 Å, corresponding to the presence of hydrogen, as well as lines at 3888.00 and 5875.00 Å, corresponding to helium.

E. Gemini

1. Castor (α-Geminorum)

Like Capella, Castor is hard to "read into" since it consists of three gravitationally bound stars, Castor A, B, and C.[24] Castor A is the brightest and the most massive of these three, helping give the overall system a type-A main-sequence identity. Our expectation to find hydrogen absorption lines (typical of type-A stars) was fulfilled: we found a total of five hydrogen Balmer lines. However, Castor B, a metallic line star, also contributes (somewhat) to the spectrum, inspiring us to look for calcium absorption lines.

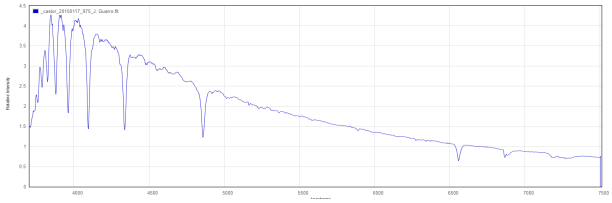

Figure XVI.[25] Above is the spectrum of Castor found on the British Astronomical Association’s database clearly shows the presence of hydrogen absorption lines. The shorter wavelengths show some absorption features reminiscent of the closely-spaced calcium absorption lines.

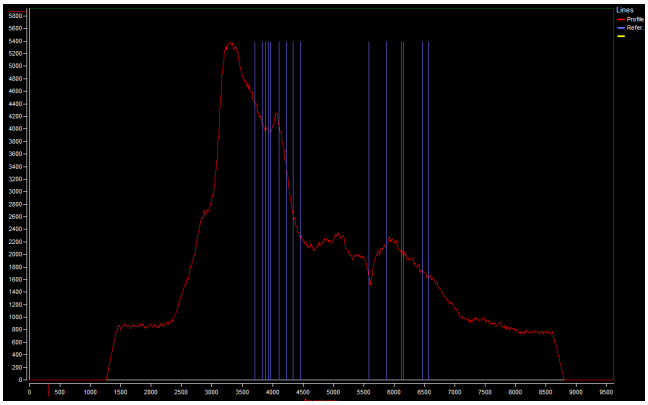

Figure XVII. Above is our spectrum of Castor. We observed hydrogen Balmer absorption lines at 3835.38, 3970.07, 4101.74, 4340.47, and 6562.81 Å, helium absorption lines at 3888.00 and 5875.00 Å, both of which were more likely Castor A’s contributions. Castor B’s contributions are fainter, but small absorptions at shorter wavelengths can be matched to calcium absorption (try zooming in). Specifically, we believe there to be absorption due to calcium at the following wavelengths: 3706.03, 3933.66, 4226.73, 4456.61, 5588.76, 6122.22, 6162.17, and 6462.57 Å.

2. Pollux (β-Geminorum)

The spectrum of Pollux is more straightforward than Castor’s, as Pollux is a single star. A type-K giant, we expect Pollux to feature hydrogen and helium lines, as well as traces of heavy elements.[26] Unfortunately, we were unable to find traces of heavy elements because the spectrum was featureless aside from the hydrogen and helium features.

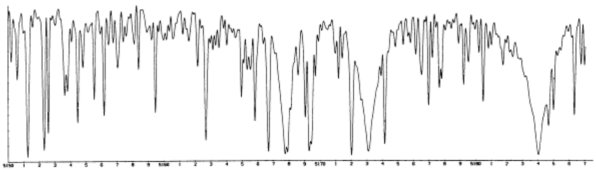

Figure XVIII.[27] Above is the spectrum of Pollux found by Ruland et al. in their paper *Spectroscopic analysis of Pollux relative to the sun with special reference to Arcturus*. The spectrum likely reflects the presence of many of the heavy elements described above, but our spectra was in this regard featureless.

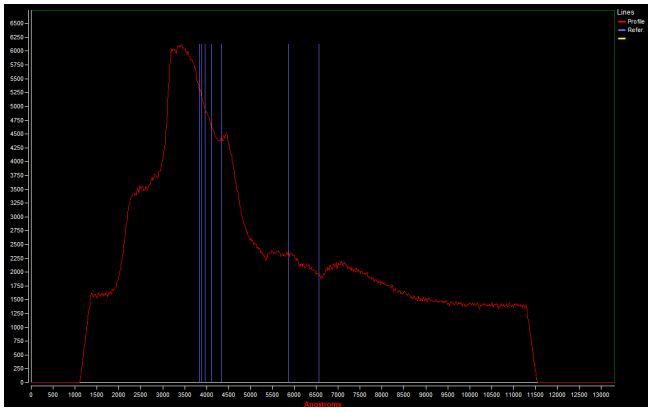

Figure XIX. Above is our spectrum of Pollux. We identified two absorption lines at 3888.00 and 5875.00 Å corresponding to helium, and four absorption lines at 3835.38, 3970.07, 4101.74, 4340.47, and 6562.81 Å corresponding to hydrogen.

F. Canis Major

1. *Sirius (α-Canis Majoris)*

Lastly, we analyze the spectrum of the brightest star in the night sky: Sirius. Sirius is a double star, but Sirius A dramatically outshines white dwarf Sirius B, so we can safely confine our findings to the former. Like Pollux, Sirius is enriched with heavy elements,[28] but our apparatus was not sensitive enough to pick up the signatures of these elements.

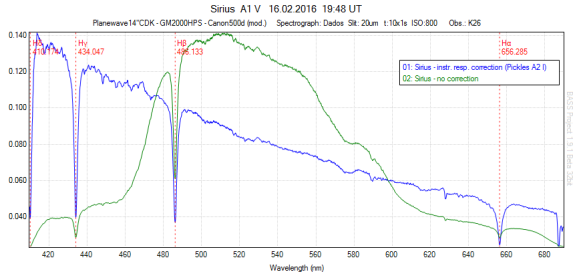

Figure XX.[29] Above is the spectrum of Sirius found on Raymond Kneip's My Astro-Page. The spectrum reveals four major absorption features characteristic of hydrogen Balmer lines. Note the x-scale is in nanometers, not angstroms.

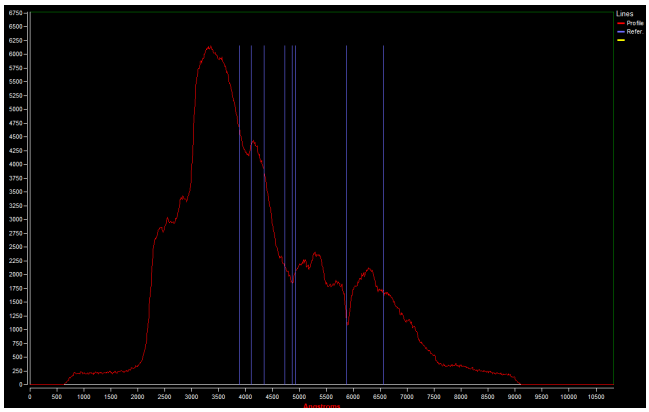

Figure XXI. Above is our spectrum of Sirius. We see absorption lines at 3888.00, 4723.00, 4921.00, and 5875.00 Å characteristic of helium, as well as lines at 4101.74, 4340.47, 4861.33, and 6562.81 Å characteristic of hydrogen.

V. CONCLUSION

We have verified the primary contents of thirteen stars in the winter sky by spectroscopic means. Unfortunately, the existence of heavy elements in stars like Sirius and Pollux could not be verified due to the physical limitations of our apparatus. Below we discuss three sources of error that, if improved, would lead to the detection of these heavy elements and improve the clarity of the already-detected spectroscopic features.

A. Focus

The focal knob of the Tasco Newtonian reflector does not allow for fine focal corrections. Thus our spectra were all slightly out-of-focus, resulting in less "sharp" spectroscopic features. Finer features (like those due to the presence of heavy elements) were "blurred out" altogether, so a more precise focal knob (or a fine tuning knob) would allow for the detection of such features.

B. Stability

The telescope was mounted on a flimsy, plastic altitude-azimuth mount, making it susceptible to minor environmental perturbations (like wind, vibration due to stepping near the telescope, etc.). These perturbations lasted within the exposure time (up to .7 seconds), causing the spectra to blur. The effects of this blurring are similar to those described above: finer features are lost and already-detected features are made less prominent. A higher-quality stand would easily solve this problem.

C. Exposure

High-quality spectrometry is always performed using long exposure. However, in order to capture long exposures, the telescope must track along with the apparent motion of the celestial sphere (the rotation of Earth). The Tasco Newtonian telescope had no such capabilities, making long-exposure spectroscopy impossible. Longer exposures of spectra allows the CCD to integrate over more time, leading to a greater photon count with less noise or statistical error. All of the professional spectra displayed in this paper were captured using long exposures, revealing many of the finer details we missed.

AUTHOR CONTRIBUTIONS

C.G. collected and analyzed the data, A.W. and A.J. gathered sources and compared the experimental results to literature, and A.W., A.J., and C.G. wrote the report.

ACKNOWLEDGEMENTS

Ian Grey

Our team thanks Ian Grey for generously lending us his fine diffraction grating and for guiding us through the beginnings of this project.

Tom Field

C.G. thanks Tom Field, President of Field Tested Systems LLC and Contributing Editor of *Sky & Telescope Magazine*, for helping with technical difficulties in `RSpec` and providing guidance on the analysis of our first spectra.

David Taylor

Our team thanks David Taylor for repairing various issues with the tracking mechanism of UTD's C8 telescope.

Parents

C.G. thanks his parents for letting him store bulky telescope equipment in their home.

SOURCES

[1] Olivier Darrigol. *A History of Optics from Greek Antiquity to the Nineteenth Century.* Oxford University Press. 2012. (81).
[2] Hearnshaw, J.B. *The analysis of starlight.* Cambridge: Cambridge University Press. 1986. (27).
[3] In fact, looking for temporal periodicity in the spectra "host stars.
[4] J.J. Sakurai. *Modern Quantum Mechanics*, 2nd ed. Cambridge University Press. 2017. 80-88.
[5] For a full development on this topic, refer to J.J. Sakurai's *Modern Quantum Mechanics*, section 2.7 in the edition cited above.
[6] David Griffiths. *Introduction to Quantum Mechanics*, 2nd ed. Pearson. 2015. 25-26.
[7] See Griffiths' *Introduction to Quantum Mechanics* section 9.3 for a great treatment of this topic.
[8] Griffiths' *Introduction to Quantum Mechanics* section 9.1.
[9] Williams College Astronomy page.
[10] Jim Kaler. *ALDEBERAN (Alpha Tauri).*
[11] British Astronomical Association: Alpha Tau.
[12] Jim Kaler. *ELNATH (Beta Tauri).* STARS. University of Illinois.
[13] Jim Kaler. STARS. University of Illinois.
[14] Jim Kaler. *ALPHERATZ (Alpha Andromedae).* STARS. University of Illinois.
[15] British Astronomical Association: alf Ori.
[16] Jim Kaler. *RIGEL (Beta Orionis).* STARS. University of Illinois.
[17] British Astronomical Association: Rigel.
[18] Jim Kaler. *BELLATRIX (Gamma Orionis).* STARS. University of Illinois.
[19] Jim Kaler. *MINTAKA (Delta Orionis).* STARS. University of Illinois.
[20] Jim Kaler. *ALNILAM (Epsilon Orionis).* STARS. University of Illinois.
[21] Jim Kaler. *ALNITAK (Zeta Orionis).*
[22] Jim Kaler. *CAPELLA (Alpha Aurigae).*
[23] British Astronomical Association: alf Aur.
[24] Jim Kaler. *CASTOR (Alpha Geminorum).*
[25] British Astronomical Association: CASTOR.
[26] Jim Kaler. *POLLUX (Beta Geminorum).*
[27] Ruland, F., Holweger, H., Griffin, R., Griffin, R. F., Biehl, D. *Spectroscopic analysis of Pollux relative to the sun with special reference to Arcturus.* Astronomy and Astrophysics, vol. 92, no. 1-2, Dec. 1980, p. 70-85.
[28] Jim Kaler. *SIRIUS (Alpha Canis Majoris).*
[29] Raymond Kneip. *My Astro-Page: Stellar spectra.*